ResearchGate

See discussions, stats, and author profiles for this publication at: https://www.researchgate.net/publication/258675791

Measurement of the 13C/12C of Atmospheric CH4 Using Near-IR Cavity Ring-Down Spectroscopy

ARTICLE · OCTOBER 2012

READS
21

10 AUTHORS, INCLUDING:

Kevin Lehmann
University of Virginia
244 PUBLICATIONS **5,920** CITATIONS
SEE PROFILE

Barbara Sherwood Lollar
University of Toronto
154 PUBLICATIONS **4,438** CITATIONS
SEE PROFILE

Georges Lacrampe-couloume
University of Toronto
94 PUBLICATIONS **2,418** CITATIONS
SEE PROFILE

Available from: Kevin Lehmann
Retrieved on: 01 February 2016

analytical chemistry

Article

pubs.acs.org/ac

Measurement of the $^{13}C/^{12}C$ of Atmospheric CH_4 Using Near-Infrared (NIR) Cavity Ring-Down Spectroscopy

Y. Chen,*[,†] Kevin. K. Lehmann,[‡] J. Kessler,[§] B. Sherwood Lollar,[▽] G. Lacrampe Couloume,[▽] and T. C. Onstott[†]

[†]Department of Geosciences, Princeton University, Princeton, New Jersey 08544, United States

[‡]Department of Chemistry, University of Virginia, Charlottesville, Virginia 22904, United States

[§]Department of Earth and Environmental Sciences, University of Rochester, Rochester, New York 14627, United States

[▽]Department of Earth Sciences, University of Toronto, Toronto, Ontario, Canada M5S 3B1

ABSTRACT: A near-infrared (NIR) continuous-wave-cavity ring-down spectrometry (CW-CRDS) device was developed with the goal of measuring seasonal changes in the isotopic composition of atmospheric CH_4 on Earth and eventually on Mars. The system consisted of three distributed feedback laser diodes (DFB-LDs), two of which were tuned to the absorption line peaks of $^{12}CH_4$ and $^{13}CH_4$ at 6046.954 cm^{-1} and 6049.121 cm^{-1}, respectively, and a third that measured the baseline at 6050.766 cm^{-1}. The multiple laser design improved the long-term stability of the system and increased the data acquisition rate. The acquisition frequency was further increased by utilizing a semiconductor optical amplifier (SOA) to initiate cavity ring-down events. The high repetition rate combined with the superhigh reflectivity mirrors yielded precise isotopic measurements in this NIR region, even though the line strengths of CH_4 in this region are 200 times weaker than those of the strongest mid-IR absorption bands. The current system has a detection limit of 1.9×10^{-12} cm^{-1}, corresponding to 10 pptv of CH_4 at 100 Torr. For ambient air samples that contained 1.9 ppmv CH_4, the $\delta^{13}C$ of the CH_4 was determined to be $-48.7 \pm 1.7‰$ (1σ).

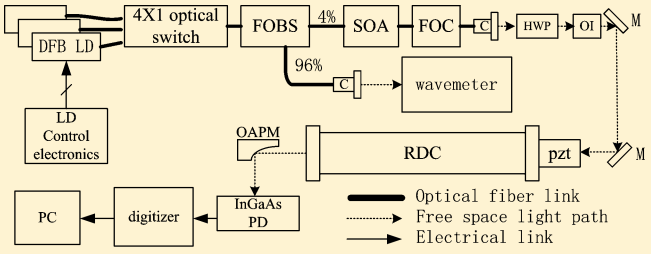

Methane (CH_4) is an important trace gas both in geosciences and astronomy. CH_4 exists in the atmosphere of six planets and Titan, with concentrations ranging from 3% to a few ppb.[1] It has been observed on an extrasolar planet[2] and in an interstellar cloud.[3] On Earth, CH_4 is a potent greenhouse gas next to CO_2 and H_2O. Seasonal releases of terrestrial CH_4 are recorded in the arctic[4] and microbial processes explain the temperature sensitive temporal pattern of its release. The determination of the isotopic composition of atmospheric CH_4 in the field and in airborne surveys will provide valuable insight on the sources of CH_4 emissions and will improve the accuracy of the predictions made by global climate models.

The isotope ratio mass spectrometry (IRMS) device is the standard instrument for isotopic analyses of CH_4. The stable carbon isotopic composition is defined, with respect to a standard, by the relation

$$\delta^{13}C = \left(\frac{\left(^{13}CH_4/^{12}CH_4\right)_{sample}}{\left(^{13}CH_4/^{12}CH_4\right)_{VPDB}} - 1 \right) \times 10^3$$

where VPDB stands for the Vienna Pee Dee Belemnite standard. For measurement of the $\delta^{13}C$ of atmospheric CH_4, preconcentration of typically 2 L of air to a volume as small as 5 mL is required,[5] and by this method, a long-term precision of ±0.2‰ is attainable.[6] The mass spectrometer must also be coupled to a gas chromatography (GC) system, to separate the CH_4 from other gases prior to oxidation to CO_2 and measurement of the carbon isotope composition. For field measurements in remote regions of the planet, for measurements performed during aerial surveys, or for planetary missions, however, weight restrictions and power requirements prohibit deploying this type of instrument.

Cavity ring-down spectroscopy (CRDS) grew out of the development of highly reflective dielectric mirrors in the mid-1980s and the necessity of being able to precisely measure their reflectivity. The tenths-of-a-kilometer path lengths created by the cavities, combined with precise measurement of the ring-down rate after turning the laser off, enabled detections limits of a few ppbs for any trace gas in the cavity.[7] This makes CRDS ideal for stable isotope analyses where the precision of the isotope ratio depends on the accurate measurement of a minor species which has an absorption peak that is distinct from that of the major species. For these reasons, instruments based on CRDS techniques have recently been developed for measuring the C isotopic composition of CH_4. Dahnke et al.[8] reported the measurement of the $\delta^{13}C$ of CH_4 in ambient air using a mid-IR

Received: May 29, 2013
Accepted: October 25, 2013
Published: October 25, 2013

 © 2013 American Chemical Society

continuous wave-cavity ring-down spectrometry (CW CRDS) device, with a precision of ±11‰ with a potential for further improvement. More recently, commercial instruments based on tunable laser absorption spectrometry and employing cavity-enhanced techniques have achieved more reproducible results under field conditions. Picarro, Inc. advertises an NIR CRDS device with a precision of ±0.8‰ for the $\delta^{13}C$ of CH_4 with a concentration as low as 20 ppmv.[9] Los Gatos Research, Inc. offers an off-axis, integrated cavity output spectrometry (OA-ICOS) device, for which they claim a precision of < ± 1‰ for an unspecified concentration CH_4.[10] For a mid-IR multipath tunable laser spectrometer, Webster[11] claimed a precision of ±10‰ for the $\delta^{13}C$ of 3 ppmv CH_4. A version of this instrument is currently on the Curiosity rover on Mars where its 1σ detection limit is 1.5 ppbv.[12]

Instrument sensitivity is determined to be first order by the effective absorption path length, which can be estimated by $L/(1 - R)$, where L is the length of the cavity and R is the reflectivity of the mirror.[13] CH_4 has its strongest absorption band near 3000 cm^{-1}.[14] In this region, mirror reflectivity can be up to 99.97%, which, for a 1-m-long cavity, corresponds to an effective absorption path length of 3.3 km. Although the NIR region (bands near 6050 cm^{-1}) CH_4 line strengths are ∼200 times weaker than those of the mid-IR region, according to HITRAN database,[14] much higher reflectivity mirrors are available (>99.9994% at 1.650 μm). As a result, a 1-m-long cavity will yield an effective optical path of 167 km. Thus, the weaker line intensity of the analyte in the NIR region can be compensated, to a large degree, by the correspondingly higher reflectivity of the cavity mirrors. The NIR lasers and optics are also more robust under harsh working conditions than those working at the mid-IR region. The reliability of NIR semiconductor lasers has been proven in the telecommunication industry as well as scientific research, says space exploration tasks. Furthermore, the NIR optical components are not as brittle as those of the mid-IR region. For these reasons, we focused on the development of a NIR CRDS system capable of direct stable isotope analysis of atmospheric CH_4 on Earth.

EXPERIMENTAL SECTION

The light source consisted of three DFB-laser diodes (NEL NLK1U5EAAA; the output power was ∼14 mW when the driving current was 100 mA), which were responsible for measuring the ring-down times for the baseline, the $^{12}CH_4$, and the $^{13}CH_4$ peaks at 6050.766, 6046.954, and 6049.121 cm^{-1}, respectively. A 4 × 1 MEMS optical switch (Agiltron LB series 4 × 1) was used to switch between lasers. The main advantage of this approach over scanning across the absorption peaks was that more time was spent measuring the absorption at its most detectable wavenumber and less time was spent waiting for the laser to stabilize to new current settings (on the order of seconds), seeking resonance conditions at different wavelengths and measuring noisier peak side data. The multiple laser design also has been proven to be an effective way to overcome the long-term instability of the CRDS and thus extends the time over which the ring-down times can be integrated.[15] This was critical to providing a precise measurement of the absorption of $^{13}CH_4$ whose concentration was typically 100 times less than that of $^{12}CH_4$.

At the output of the 4 × 1 MEMS optical switch, the light was split into two by a fiber beam splitter (FOBS) (OZ Optics) with ∼4% of the power being fed to a semiconductor optical amplifier (SOA) (Thorlabs BOA1082P with a typical gain of 16.4 db). The remainder was fed to a Bristol Instruments wavemeter (model 621A-IR) to precisely determine the wavenumber. The SOA worked as an optical amplifier as well as a switch to control injection of the laser light into the cavity. When resonance occurred the SOA shut the light off in order to generate ring-down signals in rapid succession without turning on and off the laser itself. Compared to other switching components, e.g., a free space acousto-optic modulator, the fiber SOA was easier to optically align, and it also consumed less power. The output power of the SOA was ∼11 mW.

A fiber circulator (OZ Optics, Model FOC-12P) was inserted between the SOA and the collimator. The circulator serves to block the back reflection from the front mirror to the SOA and to facilitate the alignment by maximizing the back-reflected power monitored while adjusting the front mirror of the cavity until it was normal to the optical axis. At the output of the collimator, the polarization was linear. All optical fibers were polarization maintenance type. An achromatic half waveplate (Thorlabs AHWP05M-1600) and a free space optical isolator (Thorlabs IO-4-1650-VLP) were inserted between the collimator and the front mirror of the cavity. The half waveplate was used to adjust the laser's direction of polarization to reduce the extra noise caused by birefringence of the ring-down cavity.[16] The optical isolator was used to block the back reflection from the front mirror and to prevent any reflections between the collimator and the mirror that would cause an Etalon effect (Figure 1).

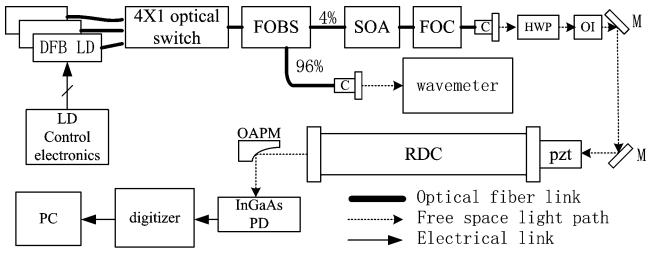

Figure 1. Schematic diagram of the experimental setup. Legend: DFB LD, distributed feedback laser diode; FOBS, fiber optics beam splitter; SOA, semiconductor optical amplifier; FOC, fiber optics circulator; c, collimator; HWP, half wave plate; OI, optical isolator, M, flat mirror; RDC, ring-down cavity; PD, photodiode; and OAPM, off-axis parabolic mirror.

The optical cavity had a length of 0.653 m with one pair of super mirrors (Advanced Thin Films), one of which was flat and the other of which had a radius of 1 m (Figure 1). One of the mirrors was actuated with three lead zirconate titanate (PZT) piezoelectric drivers to fine-tune the length of the cavity in order to bring it into resonance with the input laser. The mirrors had reflectivities of over 99.9993% at a wavelength of 1.651 μm as determined at the factory, equivalent to a 93.3 km absorption path length. An intracavity aperture with a diameter of 6 mm was inserted to eliminate resonant modes higher than TEM_{00}. At the exit of the cavity, a parabolic reflector focused the light on an InGaAs photodiode detector (Tiger Optics, Warrington, PA).

To minimize Etalon effects, all the optical surfaces have antireflection coatings and for all the surface of the optical elements we aligned them at a small angle that was not normal to the light path with the exception of the collimator. Etalon effects were further reduced by placing optical elements

dx.doi.org/10.1021/ac401605s | Anal. Chem. 2013, 85, 11250−11257

external to the cavity at Etalon immune distances, or EIDs, equal to $c/2\nu$, where ν equals the cavity's resonance frequency of transmission.[17] In this way, the free spectral range (FSR) of optical cavity was the same or multiple times the FSR of the external potential Etalon effects. Ideally, the three resonance frequencies utilized would experience the same EID and, thus, the same baseline loss. When the EID defined by the cavity could not be used by the external optical elements, the EID of the external optical surfaces was used to set the difference between $^{13}CH_4$ and baseline measurement frequencies, so that they were immune to unwanted Etalon effects.

Each laser diode's wavenumber was tuned by the combination of driving current and the temperature of the laser media, whose substrate was attached to an internal thermoelectric cooler (TEC). The current and the temperature of the laser diode were controlled by a typical voltage to current converter similar to that developed by Libbrecht and Hall,[18] except that the polarity is opposite to that of their model because the input voltage was referred to the signal ground instead of the positive power supply. The TEC controller utilized the Max1968 (Maxim Integrated, Inc.), which is a high-efficiency pulse width modulation (PWM) TEC driver. For all critical components, we applied ultralow noise and zero-drifting operational amplifiers (Model ADA4528-1, Analog Devices, Inc.), for which the temperature coefficients of the offset voltages were as low as several nv/°C. The cases of the laser diodes were mounted on an external TEC temperature controller to further stabilize their temperature. The standard deviation of the wavenumber for the laser diode was 1.7×10^{-4} cm^{-1} at a wavenumber of 6050.321 cm^{-1} for over $2^1/_2$ h. This value was the same as the measurement uncertainty of the shot-to-shot repeatability of our wavemeter and is equivalent to a long-term frequency stability of better than 5 MHz. The DFB laser driver contained two 18-bit digital-to-analog converters (AD5781, Analog Devices, Inc.) for tuning the driving current and the internal TEC temperature digitally. The equivalent lowest current resolution was 1.9 μA, which corresponded to a wavenumber step of less than 5×10^{-5} cm^{-1}.

Increasing the ring-down repetition rate is a straightforward way to improve the detection limit of the CRDS. A typical approach is to lock the laser frequency to the cavity by means of the Pound–Drever–Hall (PDH) technique[19,20] resulting in minimal dead time between the consecutive ring-downs. The repetition rate of ring-down events has been reported by Martinez et al.[19] to be over 10 kHz when the exponential decay time was 28 μs. If this scheme worked for our cavity, then the repetition rate would be over 700 Hz. Unfortunately, this scheme only works for narrow line width lasers and a relatively lower finesse cavity. For example, Paldus et al.[20] utilized an external cavity diode laser (ECL) and Martinez et al.[19] utilized a Ti:sapphire ring laser, both of which have narrower line widths than the DFB laser. Moreover, unlike the DFB laser, the frequency jittering of these lasers were mainly caused by acoustic vibration, which required a much narrower bandwidth for the feedback loop to stabilize the frequency of laser. Our DFB laser diodes had line widths of 1 MHz, whereas the cavity had a finesse of over 5×10^6 and a free spectral range (FSR) of 230 MHz. As a result, the transmission line width of the cavity was only 400 Hz, which was much narrower than the laser diode's line width. Practically, it was very difficult to lock the laser diode to such a high finesse cavity with the PDH technique. Instead, we modified the PZT scanning pattern by using a low-frequency triangular waveform with high enough amplitude to search for the resonance point. This scanning range was wide enough to cover one FSR of the cavity. Once resonance was achieved, we paused the low-frequency waveform by maintaining the driving voltage of the PZT at the level at which resonance occurred and superposed on it a higher frequency driving voltage with smaller amplitude oscillations so that the PZT would scan about 1/8 of the FSR in the vicinity of the resonance point. If within 100 ms the resonance condition was lost and there were no more ring-down events due to the drift of the laser frequency or to acoustic disturbances of the cavity, the control circuitry switched back to the low frequency waveform. The scan rate of the PZT was limited by the "ring-up" time of cavity, which was equal to the ring-down time. Scan rates exceeding the ring-up time limit would result in less energy stored in the cavity, lowering the amplitude of the waveform and reducing the signal-to-noise ratio. The ring-down time for a $1/e$ decay in intensity was ~0.37 ms when the cavity was evacuated, which corresponds to a mirror reflectivity of 0.999994%. Within this time scale, the PZT scanned <30% full width at half maximum (fwhm) of the DFB laser diode so that the cavity longitudinal mode kept being overlapped with the laser line width. This limited the low frequency waveform to 3 Hz, and we used 25 Hz for the high-frequency waveform. With the combination of the low noise, low drift laser driver and the adaptive PZT scanning scheme, we acquired about 30 ring-downs per second with each ring-down recorded to over 6 times 1/e. The nonlinear fitting routine used to calculate the ring-down time was based on a Levenberg–Marquardt algorithm, programmed in LabView (National Instruments, Austin, TX) and required ~50 ms per ring-down.

Before being injected into the cavity, the gas sample was first loaded into an ascarite (Sigma–Aldrich Co., LLC No. 223913-NaOH coated silica gel 8–20 mesh)-bearing cartridge. The cartridge had two bellows-sealed needle valves to isolate it from the cavity and the ambient condition. The cartridge both removed CO_2 from the sample and controlled the pressure of the sample. Before the gas samples were injected, both the cartridge and the cavity, were alternatively flushed by UltraZero (UZ) Air and then evacuated by rotary vane vacuum pump several times. They were then pumped down to <0.1 Torr. The sample was first injected into the cartridge with the valve between the cavity and the cartridge, closed using a gastight syringe. The pressure of the sample was monitored by a Baratron transducer (MKS Instruments, Inc., Model 622B) during this injection and was manually adjusted, using the gas-tight syringe, to be ~780 Torr. The valve between the cartridge and the gas-tight syringe was then closed, and the valve between the cavity and the cartridge was opened. The sample then expanded into the cavity and equilibrated at ~110 ± 1 Torr where the pressure broadening was sufficiently reduced to eliminate significant peak overlaps between $^{13}CH_4$ and $^{12}CH_4$, before closing the valve. This protocol prevented isotopic fractionation of the CH_4 caused by dynamic flow. A high precision (±0.015 °C) digital thermometer (Omega Engineering, Inc., HH42) continuously monitored the cavity temperature. The reading was transferred to the computer, which ran a digital proportional–integral–differential (PID) scheme to control a PWM heater controller that stabilized the temperature of the cavity at 30 ± 0.05 °C.

To measure the absorbance values of $^{13}CH_4$ and $^{12}CH_4$, we first switched to the 6050.766 cm^{-1} laser and recorded 50 ring-downs of the baseline, then we switched to the 6049.121 cm^{-1} laser and recorded 50 ring-downs of $^{13}CH_4$ peak and then we

switched to the 6046.954 cm^{-1} laser and recorded 5 ring-downs of $^{12}CH_4$ peak. Since the $^{12}CH_4$ peak's absorbance was much larger than that of the $^{13}CH_4$ peak, we assigned less measurement time to it. From the average of these ring-down times, we determined the $\overline{\tau}_0$, $\overline{\tau}_{^{13}C}$, and $\overline{\tau}_{^{12}C}$, respectively. The absorbance (α) of the $^{12}CH_4$ and $^{13}CH_4$ were then calculated by the following equations:

$$\alpha_{^{12}CH_4} = \frac{1}{c}\cdot\left(\frac{1}{\overline{\tau}_{^{12}C}} - \frac{1}{\overline{\tau}_0}\right) \quad (1)$$

$$\alpha_{^{13}CH_4} = \frac{1}{c}\cdot\left(\frac{1}{\overline{\tau}_{^{13}C}} - \frac{1}{\overline{\tau}_0}\right) \quad (2)$$

where $\overline{\tau}_{^{12}C}$ is the average 1/e ring-down time for the $^{12}CH_4$ peak (μs), $\overline{\tau}_{^{13}C}$ the average 1/e ring-down time for the $^{13}CH_4$ peak (μs), and $\overline{\tau}_0$ is the baseline 1/e ring-down time (μs); in these measurements, α is given in cm^{-1} and c is the speed of light (29 979.2 cm μs^{-1}). We refer to this measurement procedure as the multichannel chopping scheme.

We selected 6050.766 cm^{-1} for the baseline measurement in order to avoid interference from other gas species. The difference between mirror reflectivity for this wavenumber and for the wavenumber of $^{13}CH_4$ at 6049.121 cm^{-1}, however, contributed an apparent absorbance as high as 1×10^{-10} cm^{-1}, which was almost 10% of the absorbance of $^{13}CH_4$ in ambient air. To correct for this systematic error, we flushed the cavity several times with UZ Air (Airgas, Inc.), which contained a few ppbv of $^{12}CH_4$ and, thus, a few tens of pptv of $^{13}CH_4$. We then filled the cavity to the same pressure with UZ Air as was used during sample analyses and measured the α values of the $^{12}CH_4$ and $^{13}CH_4$ peaks using the same multichannel chopping scheme. The reflectivity differences at the $^{12}CH_4$ and $^{13}CH_4$ peaks, and baseline wavenumbers and the trace amount of CH_4 in the UZ Air contribute to these α values. We then subtracted these two α values from the sample's $^{12}CH_4$ and $^{13}CH_4$ α values to determine the "true" absorbance ratio of the sample. We found this method for determining the true absorbance ratio of the samples was more accurate and reproducible than measuring the difference in the ring-down times of the $^{12}CH_4$ and $^{13}CH_4$ peaks and baseline of the sample versus the evacuated cavity. Since our HR mirrors also simultaneously served as the seals for the cavity by pressing against on Viton O-rings, they always experienced a pressure difference of a few hundred Torr between the inside and the outside of the cavity. Because this stress on the mirrors causes slight changes in their reflectivity the background correction procedure should replicate the same pressure used during analysis of the samples. The agreement in the 'true' absorbance ratio for the same CH_4 standard diluted to different concentrations with UZ air demonstrates the validity of this baseline correction procedure and that the isotopic composition of the CH_4 in the UZ Air has no significant impact (Figure 2).

If the spectral line strength of each absorption line were known very precisely then they could be used to determine the isotope ratio, but the absolute line strength is a function of temperature and line broadening depends on both temperature and pressure. The line strength predicted by computation from the HITRAN database parameters has an uncertainty much larger than that required for stable isotope analysis. An alternative way is to subsequently measure the absorbance ratio of $^{13}CH_4$ and $^{12}CH_4$ for a sample and a standard CH_4 under the same temperature and pressure. The $\delta^{13}C$ of the sample is then given by the expression:

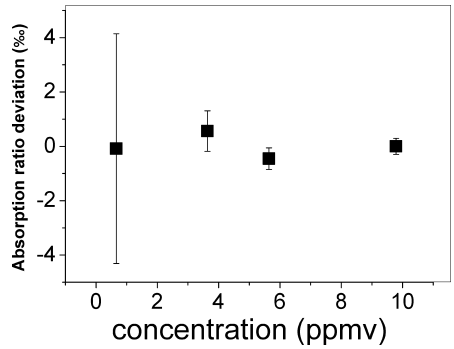

Figure 2. The difference between the $^{13}CH_4$ to $^{12}CH_4$ absorption ratio of Standard42 CH_4 diluted in UZ air for various concentrations, compared to the absorption ratio of Standard42 at the highest concentration of 10 ppmv. The error bars were calculated using eq 5 and represent $\pm 1\sigma$.

$$\delta^{13}C_{sample} = \frac{\overline{R}_{\alpha,sample} - \overline{R}_{\alpha,stand}}{\overline{R}_{\alpha,stand}} \times (1000 + \delta^{13}C_{standard}) + \delta^{13}C_{standard} \quad (3)$$

where the absorbance ratio $R_\alpha = \alpha_{^{12}C}/\alpha_{^{13}C}$ and $\delta^{13}C_{standard}$ is the carbon isotope composition of the CH_4 standard versus the VPDB standard.

From eqs 1, 2, and 3, the error of the absorbance ratio (σ_R) is given by the following expressions:

$$\sigma_\alpha = \frac{1}{c}\sqrt{\frac{\sigma_\tau^{\,2}}{\tau^4} + \frac{\sigma_{\tau_0}^{\,2}}{\tau_0^{\,4}}} \quad (4)$$

$$\sigma_R = R_\alpha \times \sqrt{\frac{\sigma_{^{13}C}^{\,2}}{\alpha_{^{13}C}^{\,2}} + \frac{\sigma_{^{12}C}^{\,2}}{\alpha_{^{12}C}^{\,2}}} \quad (5)$$

where σ_α is the error of the absorbance for the $^{12}CH_4$ and $^{13}CH_4$ peaks.

If we regard the measurements of the absorbance ratio for a sample's CH_4 peak and a CH_4 standard as independent, then the final relative error of $\delta^{13}C$ is given by

$$\frac{\sigma_{\delta^{13}C}}{\delta^{13}C} = \sqrt{\left(\frac{\sigma_{R_{sample}}}{R_{sample}}\right)^2 + \left(\frac{\sigma_{R_{standard}}}{R_{standard}}\right)^2} \quad (6)$$

The two CH_4 standards used in this study were measured at the University of Toronto by gas chromatography–combustion–isotope ratio mass spectrometry (GC-C-IRMS), using a Varian 3400 gas chromatograph attached to Finnigan Mat 252 mass spectrometer through a combustion interface. The CH_4 was injected into an Agilent GSQ capillary column 60 m long and 0.32 mm in inner diameter (ID). The GC oven was at 35 °C and the He flow was 1.5 mL min^{-1}. At the end of the column, the CH_4 was oxidized to H_2O and CO_2 in a 30-cm-long by 0.8-mm-ID alumina tube with three CuO wires and one NiO wire. To ensure full conversion of CH_4, the alumina tube temperature was regulated at 940 °C. The H_2O was removed from the gas mixture by passing it through a Naphion membrane tube with an ultradry He reverse flow. The He and CO_2 mixture was introduced into the mass spectrometer

dx.doi.org/10.1021/ac401605s | Anal. Chem. 2013, 85, 11250–11257

and the carbon isotope ratio was determined by comparison with a CO_2 gas standard stored in the internal bellow of the dual inlet of the mass spectrometer.[21] The CO_2 gas standard (secondary standard) was anchored by dual inlet analysis to the NBS 18 and NBS 19 carbonates international standards (primary standards) with a precision of 0.05‰ through the procedures described in the International Atomic Energy Agency report (No. IAEA-TECDOC-825) and references therein.[22]

The isotope ratio values (−44.5‰ and −42.3‰VPDB) were determined by the average of more than 50 GC-C-IRMS analyses. Taking into account reproducibility and accuracy, the standard error (1σ) was 0.25‰. In the following section, "Standard44" and "Standard42" denote the CH_4 standards that have $\delta^{13}C$ values of −44.5‰ and −42.3‰, respectively. Standard44 was diluted to about 6.8 ppmv CH_4 with UZ Air before CRDS analysis. A dilution series of 1.8, 5.1, 8.7, and 12.1 ppmv CH_4 was prepared by mixing Standard42 and UZ air.

The $\delta^{13}C$ values determined by CRDS were calculated by referring to the absorbance ratio of Standard44 in eq 3. All standard and air samples were stored in Tedlar sample bags (SKC, Inc.) prior to measurement.

To determine the optimal integration time for the current system, we utilized an Allan variance plot to determine the number of consecutive ring-downs with the lowest mean variance. Allan variance was first developed to estimate the long-term stability of the atomic frequency standard[23] and later was utilized to study the effect of system drifting on the optimal integration time[15] for tunable laser spectroscopy.[24] The Allan variance of our CRDS was estimated based on the absorbance measurement of $^{13}CH_4$ because the absorbance measurement of $^{13}CH_4$ is more critical to precise isotopic ratios than the measurement on $^{12}CH_4$ absorbance due to the much lower concentration of $^{13}CH_4$. The Allan variance was calculated using a MatLab program and plotted versus the number of ring-downs on a $\log_{10}$ scale.

RESULTS AND DISCUSSION

Optimal Integration Time for the CRDS System and the Detection Limit Estimation. By the best effort of alignment, the standard deviation of the ring-down time constant was as low as 0.02% for the evacuated cavity. We performed 32 000 measurement cycles, each cycle containing 20 consecutive ring-downs for the baseline and for the $^{13}CH_4$ peak. The Allan variance plot indicated that the optimal number of measurements for $^{13}CH_4$ was ∼5000 (Figure 3). As a result, a measurement routine consisting of 100 cycles of 50 ring-downs on $^{13}CH_4$ and on the baseline, respectively, and 5 ring-downs on $^{12}CH_4$ was adopted. With the current ring-down repetition rate this measurement routine for the isotopic composition required ∼12 min. The detection limit was estimated to be 1.9×10^{-12} cm^{-1}, which is significantly better than the 4.4×10^{-12} cm^{-1} reported by Huang and Lehmann[15] and corresponds to a concentration of ∼10 pptv of 100 Torr CH_4. The improvement is mostly likely due to the stabilization of the laser wavelength, the longer cavity (65 cm vs 40 cm for Huang and Lehmann[15]) and higher reflectivity of the mirrors.

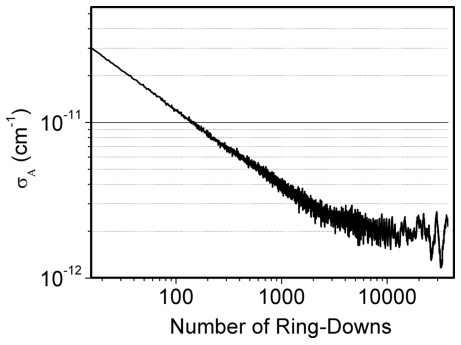

Figure 3. Allan variance plot of the error in the absorbance of $^{13}CH_4$ as a function of the number of ring-downs.

Spectrum of CH_4 Isotopes in the Near-Infrared (NIR) Region. The wavenumber of 6046.9546 cm^{-1} used for $^{12}CH_4$ represents one of the most strongly absorbing peaks in the high-reflectivity range of the mirror (Figure 4). At the ambient

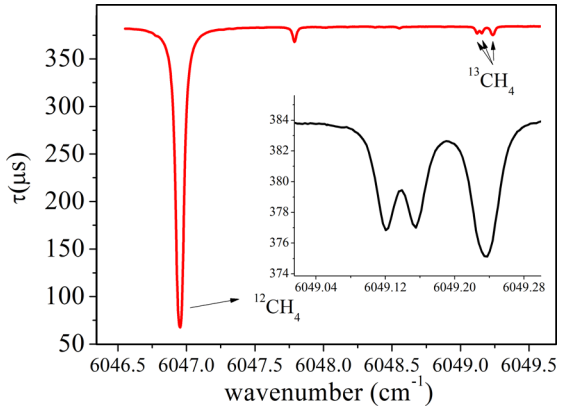

Figure 4. The CRD spectrum of $^{12}CH_4$ and $^{13}CH_4$ of outdoor air, the concentration of CH_4 was 1.9 ppmv, at 100 Torr at 21 °C. The sample went through an ascarite cartridge to remove CO_2.

laboratory temperature of 21 °C and a pressure of 100 Torr, the wavenumber of 6049.121 cm^{-1} used for $^{13}CH_4$ represents the middle line strength of the triple peaks in this region and was selected because it was least affected by overlap from a weakly absorbing trace gas contaminant believed to be CO_2. At the same temperature and pressure, a calibrated absorbance coefficient for the $^{12}CH_4$ spectral line at 6046.9546 cm^{-1} was determined to be 2.096×10^{-10} cm^{-1} $ppbv^{-1}$. One air sample measured at 21 °C and 100 Torr yielded absorbance values for $^{12}CH_4$ and $^{13}CH_4$ of $4.0266 \pm 0.0003 \times 10^{-7}$ cm^{-1} and $1.756 \pm 0.002 \times 10^{-9}$ cm^{-1} (average of 100 measurement cycles), respectively. So the concentration of the laboratory air CH_4 in above sample was 1.92 ppmv.

Systematic Stability Analysis and Absorbance Ratio of CH_4 in Ambient Air. In order to evaluate the long-term stability of the system beyond the optimal integration time, we loaded the cavity with outdoor air and performed $^{13}CH_4/^{12}CH_4$ absorbance ratio measurements on the same sample repeatedly for over 12 h, and the deviation was calculated by comparing to the individual absorbance ratio value to the average absorbance ratio of the total data points (Figure 5). Over 2 h, the standard deviation was ±0.9‰. Over 12 h of observation, the standard deviation increased to ±1.4‰ (Figure 5). This value is somewhat higher than the result predicted based on the minimum Allan variance. The exact reason for the long-term drifting is not quite clear. Ambient temperature and pressure fluctuations in the laboratory may play a role, even though the cavity was temperature-stabilized. However, the mounts of the mirror were exposed to ambient conditions and the mirrors

dx.doi.org/10.1021/ac401605s | Anal. Chem. 2013, 85, 11250−11257

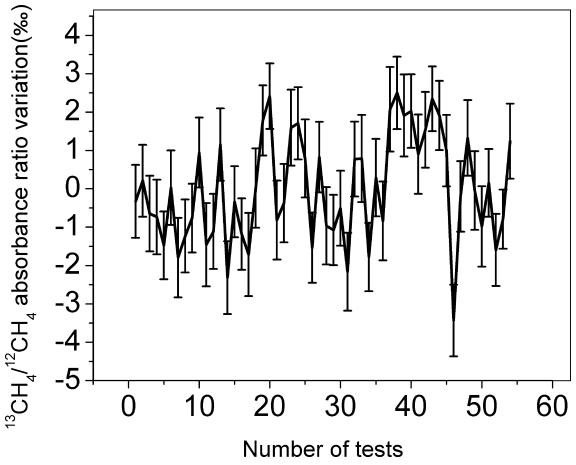

Figure 5. Long-term stability of the absorbance ratio of $^{13}CH_4/^{12}CH_4$ for one outdoor air sample being injected to the cavity, which contains 1.9 ppmv CH_4. The deviation was calculated by comparing to the individual absorbance ratio value to the average absorbance ratio of the total data points. Error bars calculated according to eq 5 and represent $\pm 1\sigma$.

themselves were virtually thermally isolated, with respect to the wall of the cavity, and their outside surfaces were exposed to the ambient conditions. Thus, the mirrors were experiencing temperature difference of ~10 °C and pressure difference of a few hundred Torr between their inner and outer surfaces. The stress and temperature fluctuation would cause the reflectivity variance.[25] If these effects are not homogeneous over different wavelengths, then the drift in the ring-down times for peaks and baseline would not be correlated and would not be canceled by our multichannel chopping measurement scheme. The ambient temperature and pressure fluctuation could also cause the mirror misalignment, which would induce the drifting of the ring-down time constant. Tang et al.[26] have shown that encapsulation of the mirrors by extra windows eliminates the pressure-induced stress and isolates them from the ambient conditions and, thus, further improves the long-term stability. Another possible reason is that a residual Etalon effect may still be present even after applying all the methods described above.

The $\delta^{13}C$ values for ambient air and standard CH_4 gases were calculated using eq 3 and the average absorbance ratio of the first Standard44 measurement, which was 0.004168. All the other $\delta^{13}C$ were calculated by comparing to this value . Each data point plotted in Figure 6 represents a fresh loading of the same sample into the cavity, except for the plot of Standard42,

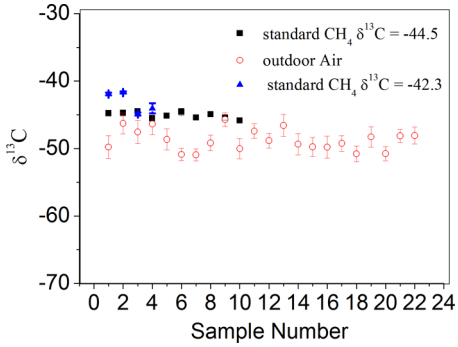

Figure 6. $\delta^{13}C$ of ambient air and the standard CH_4. Error bars calculated according to eq 6 and represent $\pm 1\sigma$.

of which each data point represent the dilution of different concentration (1.8, 5.1, 8.7, and 12.1ppmv). All data were measured within one week. The overall relative error for the absorbance ratio of atmospheric CH_4 was ±1.7‰, indicating good long-term stability. For short-term measurements (2 h), the standard deviation was ±1.3‰. For Standard44, this error is less than ±0.5‰. By eq (6), we estimated the long-term random error of the $\delta^{13}C$ to be ±1.8‰ (1σ), and the short-term random error to be ±1.4‰ (1σ) for atmospheric CH_4. By increasing the concentration of the standard CH_4, we further reduced the error of $^{13}CH_4$ absorbance.

According to the HITRAN database, the temperature coefficient for line strength ratio is ~3‰ °C^{-1} and the best we could achieve with our current instrument was ±0.05 °C. So we estimate that the best precision for the standard CH_4 will be ~0.2‰. Under this circumstance, the best precision for $\delta^{13}C$ would be the same as the precision of the absorbance ratio of the atmospheric CH_4. The systematic error would depend on the accuracy of the $\delta^{13}C$ of the standard CH_4, which, in our case, could be as good as 0.25‰.

We compared the absorbance ratio error estimated by two ways: one was starting with the uncertainty of ring-down time and using eqs 4 and 5; the other was calculated from the absorbance ratio for each measurement cycle and their estimated standard deviation. The first one indicates the precision we could achieve without multichannel chopping scheme. Take the first measurement on air CH_4 for example, the mean ring-down times for the $^{13}CH_4$ and $^{12}CH_4$ peaks and at the baseline were 333.3 ± 0.1, 65.58 ± 0.02, and 339.4 ± 0.1 μs, respectively. The uncertainties here were standard deviation of the mean τ over 100 measurement cycles. The uncertainties consisted of the long-term drifting of the ring-down time and the shot-to-shot variation. From eqs 4 and 5, we estimate the relative error of absorbance ratio σ_R/R was ±2.3‰. By multichannel chopping scheme, the relative error of absorbance ratio σ_R/R was 1.7‰; another more precise measurement on air yielded 1.4‰ vs 0.9‰. That means the optimal integration time of the system can be elongated approximately twice by the multiple-channel chopping scheme.

For both air samples and standard CH_4, the error bars were less than the standard deviation between different sampling loadings. One explanation was that disturbance of the mirror alignment could not be avoided during the evacuation of the cavity and reintroduction of a fresh sample thus introducing additional error. For CH_4 Standard42, this discrepancy was even larger and yielded a $\delta^{13}C$ value of −41.6 ± 0.2‰ for 12 ppmv, ranging down to −44.9 ± 2‰ for 1.8 ppmv (see Figure 6 and Table 1). This was probably caused by the drift of the

Table 1. $\delta^{13}C$ of Ambient Air CH_4 and Standard CH_4 Diluted with UltraZero (UZ) Air

sample	$\delta^{13}C$ by IRMS or literature (‰)	average absorbance ratio	average $\delta^{13}C$ by CRDS (‰)	standard deviation, STD (1σ), by CRDS (‰)
ambient air	from −47 to −48	0.004150	−48.7	1.7
Standard44 (6.5 ppmv CH_4)	−44.5 ± 0.25	0.004166	−45.1	0.5
Standard42 (1.8, 5.1, 8.7, and 12.1 ppmv CH_4)	−42.3 ± 0.25	0.004174	−43.1	1.6

dx.doi.org/10.1021/ac401605s | Anal. Chem. 2013, 85, 11250−11257

differential reflectivity between peaks and baseline after several days of measurement. For example, if the offset between baseline and $^{13}CH_4$ was overestimated, the lower concentration samples would yield lower $\delta^{13}C$ values. This phenomenon also occurs on commercial instruments where the long-term (e.g., 24 h) testing yields significant larger uncertainty compared to short-term testing. Another possible reason was that storage of the high concentration CH_4 in a Tedlar bag over a couple of days caused isotopic fractionation, since the higher concentration 8.7 ppmv and 12.1 ppmv yielded larger $^{13}C/^{12}C$ absorbance ratios resulting in their relatively more positive $\delta^{13}C$ values of −41.6‰ and −41.9‰, respectively. As comparison, measurement on another set of diluted standard CH_4 shows good consistence on absorbance ratio (Figure 2), since they were measured with short interval. The average $\delta^{13}C$ value of the ambient air was determined as −48.7 ± 1.7‰, which is well within error of previously published ranges of values from −47.0‰ to −47.5‰.[27,28] For many geochemical applications, this level of precision is sufficient, but in order to utilize the CRDS to monitor changes in the atmospheric CH_4 isotopic composition, the precision would need to be ±0.2‰,[6] which can be achieved through preconcentration of the air sample, as the results of our dilution experiment demonstrate (Figure 2).

In the Martian atmosphere, the CH_4 concentrations reported by Mumma et al.[3] varied from <5 ppbv to 45 ppbv.[29] If we assume a 30 ppbv CH_4 concentration and assume that a molecular sieve trap will concentrate this CH_4 by a factor of 50−100,[30] then the CH_4 concentration would be 1.5−3 ppmv. If we assume that the sample is compressed to a pressure of 100 Torr, then the absorbance of the Martian CH_4 will be comparable to the ambient terrestrial atmospheric CH_4 and would yield $\delta^{13}C$ values with similar precision of ±1.7‰.

For further improvement, for example, reducing long-term drifting, we would suggest using a more rigid cavity and shielding the ring-down cavity from ambient conditions with extra optical windows.[26]

CONCLUSION

We developed a near-infrared (NIR) wavelength-stabilized, continuous wave-cavity ring-down spectrometry (CW-CRDS) system for CH_4 isotopic analyses. The multiple laser configuration and measurement scheme significantly improved the detection limit and the precision of CH_4 isotopic analyses in the NIR region. The current system has a 1σ detection limit of 1.9×10^{-12} cm^{-1}, equivalent to 10 pptv of CH_4, at 100 Torr. The standard deviation of $\delta^{13}C$ was ±1.7‰ for the ambient air CH_4. This level of precision puts this CRDS design well within the capabilities that would be required for distinguishing different atmospheric CH_4 sources on Earth and for future surface-based robotic missions to Mars.

AUTHOR INFORMATION

Corresponding Author

*E-mail: yuhengc@princeton.edu.

Notes

The authors declare no competing financial interest.

ACKNOWLEDGMENTS

This research study was supported by NASA ASTID Grant No. NNX08AX16G to T.C.O. and K.K.L.

ABBREVIATIONS

CW-CRDS = continuous wave-cavity ringdown spectrometry
DFB-LD = distributed feedback laser diodes
SOA = semiconductor optical amplifier
IRMS = isotope ratio mass spectrometry
OA-ICOS = off-axis, integrated cavity output spectrometry
MSL = Mars Science Laboratory
TEC = thermoelectric cooler
PID = proportional−integral−differential
FSR = free spectral range
PZT = lead zirconate titanate, $Pb_xZr_{1-x}TiO_3$
UZ Air = UltraZero Air

REFERENCES

(1) Pater, I. d.; Lissauer, J. *Planetary Sciences*, 2nd Edition; Cambridge University Press: Cambridge, U.K., 2010.
(2) Swain, M. R.; Vasisht, G.; Tinetti, G. *Nature* **2008**, *452*, 329−331.
(3) Lacy, J. H.; Carr, J. S.; Evans, N. J., II; Baas, F.; Achtermann, J. M.; Arens, J. F. *Astrophys. J., Part 1* **1991**, *376*, 556−560.
(4) Mastepanov, M.; Sigsgaard, C.; Dlugokencky, E. J.; Houweling, S.; Ström, L.; Mikkel, P. T.; Christensen, T. R. . *Nature* **2008**, *456*, 628−631.
(5) Merritt, D. A.; Hayes, J. M.; Des Marais, D. J. *J. Geophys. Res.* **1995**, *100*, 1317−1326.
(6) Yarnes, C. *Rapid. Commun. Mass Spec.* **2013**, *27*, 1036−1044.
(7) Lehmann, K. K.; Berden, G.; Engeln, R. In *Cavity Ring-Down Spectroscopy: Techniques and Applications*, Berden, G.; Engeln, R., Eds.; Blackwell Publishing, Ltd.: Oxford, U.K., 2009; pp 1−26.
(8) Dahnke, H.; Kleine, D.; Urban, W.; Hering, P.; Mürtz, M. *Appl. Phys. B: Laser Opt.* **2001**, *72*, 121−125.
(9) Picarro, Inc. https://picarro.app.box.com/s/27hvnt542v78xs9nog4l (accessed May 20, 2012).
(10) Los Gatos Research, Inc., http://www.lgrinc.com/analyzers/overview.php?prodid=1&type=isotope (accessed May 20, 2012).
(11) Webster, C. R. *Appl. Opt.* **2005**, *44*, 1226−1235.
(12) Webster, C. R.; Mahaffy, P. R.; Atreya, S. K.; Flesch, G. J.; Farley, K. A. In *44th Lunar Planetary Science Conference*, Houston, TX, 2013; p 1366.
(13) Moyer, E. J.; Sayres, D. S.; Engel, G. S.; Clair, J. M. S.; Keutsch, F. N.; Allen, N. T.; Kroll, J. H.; Anderson, J. G. *Appl. Phys. B: Laser Opt.* **2008**, *92*, 467−474.
(14) Rothman, L. S.; et al. *J. Quant. Spectrosc. Radiat. Transfer* **2009**, *110*, 533−572.
(15) Huang, H.; Lehmann, K. K. *Appl. Opt.* **2010**, *49*, 1378−1387.
(16) Huang, H.; Lehmann, K. K. *Appl. Opt.* **2008**, *47*, 3817−3827.
(17) Ehlers, P.; Silander, I.; Wang, J.; Axner, O. *J. Opt. Soc. Am., B* **2012**, *29*, 1305−1315.
(18) Libbrecht, K. G.; Hall, J. L. *Rev. Sci. Instrum.* **1993**, *64*, 2133−2135.
(19) Martínez, R. Z.; Metsälä, M.; Vaittinen, O.; Lantta, T.; Halonen, L. *J. Opt. Soc. Am., B* **2006**, *23*, 727−740.
(20) Paldus, B. A.; Harb, C. C.; Spence, T. G.; Wilke, B.; Xie, J.; Harris, J. S.; Zare, R. N. . *J. Appl. Phys.* **1998**, *83*, 3991−3997.
(21) Brand, W. A. *J. Mass Spectrom.* **1996**, *31*, 225−235.
(22) International Atomic Energy Agency. *Reference and Intercomparison Materials for Stable Isotopes of Light Elements*; Report No. IAEA-TECDOC-825, Vienna, Austria, 1995.
(23) Allan, D. W. *Proc. IEEE* **1966**, *54*, 221−230.
(24) Werle, P.; Mücke, R.; Slemr, F. *Appl. Phys.* **1993**, *B 57*, 131−139.
(25) Rancourt, J. D. *Optical Thin Films: User Handbook*; SPIE—The International Society for Optical Engineering: Bellingham, WA, 1996.
(26) Tang, Y.; Yang, S.; Lehmann, K. K. *Rev. Sci. Instrum.* **2012**, *83*, 043115.
(27) Quay, P. D.; et al. *Global Biogeochem. Cycles* **1991**, *5*, 25−47.

(28) Mischler, J. A.; Sowers, T. A.; Alley, R. B.; Battle, M.; McConnell, J. R.; Mitchell, L.; Popp, T.; Sofen, E.; Spencer, M. K. *Global Biogeochem. Cycles* **2009**, *23*, GB003460.
(29) Mumma, M. J.; Villanueva, G. L.; Novak, R. E.; Hewagama, T.; Bonev, B. P.; DiSanti, M. A.; Mandell, A. M.; Smith, M. D. *Science* **2009**, *323*, 1041−1045.
(30) Mahaffy, P. R.; et al. *Space Sci. Rev.* **2012**, *170*, 401−478.